

Generalizable Data-free Objective for Crafting Universal Adversarial Perturbations

Konda Reddy Mopuri*, Aditya Ganeshan*, R. Venkatesh Babu, *Senior Member, IEEE*

Abstract—Machine learning models are susceptible to adversarial perturbations: small changes to input that can cause large changes in output. It is also demonstrated that there exist input-agnostic perturbations, called universal adversarial perturbations, which can change the inference of target model on most of the data samples. However, existing methods to craft universal perturbations are (i) task specific, (ii) require samples from the training data distribution, and (iii) perform complex optimizations. Also, because of the data dependence, fooling ability of the crafted perturbations is proportional to the available training data. In this paper, we present a novel, generalizable and data-free objective for crafting universal adversarial perturbations. Independent of the underlying task, our objective achieves fooling via corrupting the extracted features at multiple layers. Therefore, the proposed objective is generalizable to craft image-agnostic perturbations across multiple vision tasks such as object recognition, semantic segmentation and depth estimation. In the practical setting of black-box attacking scenario, we show that our objective outperforms the data dependent objectives to fool the learned models. Further, via exploiting simple priors related to the data distribution, our objective remarkably boosts the fooling ability of the crafted perturbations. Significant fooling rates achieved by our objective emphasize that the current deep learning models are now at an increased risk, since our objective generalizes across multiple tasks without the requirement of training data for crafting the perturbations. To encourage reproducible research, we have released the code for our proposed algorithm at GitHub[†].

Index Terms—Adversarial perturbations, fooling CNNs, stability of Neural Networks, perturbations, universal, generalizable attacks, attacks on ML systems, data-free objectives, adversarial noise.



1 INTRODUCTION

SMALL but structured perturbations to the input, called adversarial perturbations, are shown ([1], [2], [3]) to significantly affect the output of machine learning systems. Neural network based models, despite their excellent performance, are observed ([4], [5], [6]) to be vulnerable to adversarial attacks. Particularly, Deep Convolutional Neural Networks (CNN) based vision models ([7], [8], [9], [10], [11]) can be fooled by carefully crafted quasi-imperceptible perturbations. Multiple hypotheses attempt to explain the existence of adversarial samples, viz. linearity of the models [5], finite training data [12], etc. More importantly, the adversarial perturbations generalize across multiple models. That is, the perturbations crafted for one model fools another model even if the second model has a different architecture or trained on a different subset of training data ([4], [5]). This property of adversarial perturbations enables potential intruders to launch attacks without the knowledge about the target model under attack: an attack model typically known as *black-box attacking* [13]. On the contrast, an attack model where everything about the target model is known to the attacker is called a *white-box attacking*. Until recently, all the existing works assumed a threat model in which the adversaries can directly feed input to the machine learning system. However, Kurakin *et al.* [14] lately showed that the adversarial samples can remain misclassified even if they were constructed in physical world and observed

through a sensor (e.g., camera). Given that the models are vulnerable even in physical world scenario [14], the models' susceptibility poses serious issues about their deployability (e.g., safety concerns for autonomous driving) in the real world. Particularly, in case of critical applications that involve safety and security, reliable models need to be deployed to stand against the strong adversarial attacks. Thus, the effect of these structured perturbations has to be studied thoroughly in order to develop dependable machine learning systems.

Recent work by Moosavi-Dezfooli *et al.* [8] presented the existence of image-agnostic perturbations, called universal adversarial perturbations (UAP) that can fool the state-of-the-art recognition models on most natural images. Their method for crafting the UAPs is based on the DeepFool [7] attacking method. It involves solving a complex optimization problem (eqn. 2) to design a perturbation. The UAP [8] procedure utilizes a set of training images to iteratively update the universal perturbation with an objective of changing the predicted label upon addition, for most of the dataset images. Similar to [8], Metzen *et al.* [11] proposed UAP for semantic segmentation task. They extended the iterative FGSM [5] attack by Kurakin *et al.* [14] to change the label predicted at individual pixels and craft the perturbation. They craft the image-agnostic perturbations to fool the system in order to predict a pre-determined target segmentation output.

However, these approaches to craft UAPs ([8], [11], [15]) have the following important drawbacks:

- *Data dependency*: It is observed that the objective presented by [8] to craft UAP for recognition models requires a minimum number of training samples

• The authors are with Department of Computational and Data Sciences, Indian Institute of Science, Bangalore, India, 560012.
E-mail: kondamopuri@iisc.ac.in, adityaganeshan@gmail.com and venky@iisc.ac.in

* denotes equal contribution

[†] <https://github.com/val-iisc/gd-uap>

for it to converge and craft an image-agnostic perturbation. Moreover, the fooling performance of the resulting perturbation is proportional to the available training data (Figure 4). Similarly, the objective for crafting image-agnostic perturbation for semantic segmentation models proposed by [11] also requires data. Therefore, as their optimization/objectives involve data, existing procedures can not craft perturbations when enough data is not provided.

- *Weaker black-box performance:* Since information about the target models is generally not available for attackers, it is practical to study the black-box attacks. Also, black-box attacks reveal the true susceptibility of the models, while white-box attacks provide the upper bound on the achievable fooling. However, the black-box attacking performance of UAP [8] is poor compared to their white-box performance (Table 4). Note that, in [8], authors have not analyzed the performance of their perturbations in the black-box attack scenario. They have assumed that the training data of the target models is known and have not considered the case in which adversary has access to only a different set of data. This amounts to performing only *semi white-box* attacks. Black-box attacks generally mean [13] the adversary does not have access to (i) the target network architecture (including the parameters), and (ii) a large training dataset. In case of semantic segmentation, as [11] worked with targeted attacks, they observed that the perturbations do not generalize to other models very well.
- *Task specificity:* The current objectives to craft UAPs are task specific. The objectives are typically designed to suit the underlying task at hand as the concept of fooling varies across the tasks. Particularly, for regression tasks such as depth estimation and crowd counting, the idea of fooling is not straight forward as it is for recognition task.

In order to address the above shortcomings and to better analyze the stability of the models, we present novel data-free objective to craft universal adversarial perturbations. Our objective is to craft image-agnostic perturbations that can fool the target model without any knowledge about the data distribution, such as, the number of categories, type of data (e.g., faces, objects, scenes, etc.) or the data samples themselves. Since we do not have access to any data, instead of an objective that reduces the confidence to the predicted label or flip the predicted label (as in [4], [7], [8], [11]), we propose an objective to learn perturbations that can adulterate the features extracted by the models. Our proposed objective attempts to over-fire the neurons at multiple layers in order to deteriorate the extracted features. During the inference time, the added perturbations misfire the neuron activations in order to contaminate the representations and eventually predict wrong label.

This work extends our earlier conference paper [9]. We make the following new contributions in this paper:

- 1) Propose a novel data-free objective for crafting image-agnostic perturbations
- 2) We demonstrate that our objective is generalizable across multiple vision tasks
- 3) Further, we show that apart from being data-free objective, the proposed method can exploit minimal prior information about the training data distribution of the target models in order to craft stronger perturbations
- 4) We present comprehensive analysis on the proposed objective and the crafted perturbations across three different vision tasks covering both classification and regression tasks.

The rest of this paper is organized as follows: section 2 presents detailed account of related works, section 3 discusses the proposed data-free objective to craft image-agnostic adversarial perturbations, section 4 demonstrates the effectiveness of our perturbations via comprehensive experimentation, section 5 hosts discussion on the proposed method and finally section 6 concludes the paper.

2 RELATED WORKS

Szegedy *et al.* [4] demonstrated that despite their superior recognition performance, neural networks are susceptible to adversarial perturbations. Subsequently, multiple other works [5], [6], [7], [16], [17], [18], [19] studied this interesting and surprising property of the machine learning models. Though it is first observed with recognition models, the adversarial behaviour is noticed with models trained on other tasks such as semantic segmentation [11], [20], object detection [20] and deep reinforcement learning tasks [21], etc. There exist multiple methods to craft these malicious perturbations for a given data sample. For recognition tasks, they range from performing simple gradient ascent ([5]) on cost function to solving complex optimizations ([4], [7], [22]). Simple and fast methods such as FGSM [5] find the gradient of loss function to determine the direction in the image space to perturb the input image. An iterative version of this attack presented in [14] achieves better fooling via performing the gradient ascent multiple times. On the other hand, complex approaches such as [4], [7] find minimal perturbation that can move the input across the learned classification boundary in order to flip the predicted label. More robust adversarial attacks have been proposed recently that transfer to real world [14] and are invariant to general image transformations [23].

Moreover, it is observed that the perturbations exhibit transferability property. That means, perturbations crafted for one model can fool other models with different architectures and trained on a disjoint training set as well ([4], [5]). Further, Papernot *et al.* [13] introduced a practical attacking setup via model distillation to understand the *black-box* attacking. Black-box attacking assumes no information about the target model and its training data. They proposed to use a target model’s substitute to craft the perturbations.

The common underlying aspect of all these techniques is that they are intrinsically data dependent. The perturbation is crafted for a given data sample independently of others. However, recent works by Moosavi-Dezfooli *et al.* [8] and Metzen *et al.* [11] showed the existence of input-agnostic perturbations that can fool the models over multiple images. In [8], authors proposed an iterative procedure based on

Deepfool attacking [7] method to craft a universal perturbation to fool classification models. Similarly, in [11], authors craft universal perturbations that can result in target segmentation outputs. However, both these works optimize for different task specific objectives. Also, they require training data to craft the image-agnostic perturbations. Unlike the existing works, the proposed method presents a data-free objective that can craft perturbations without the need for any data samples. Also, we introduce a generic notion of fooling across multiple computer vision tasks via over-firing the neuron activations. Particularly, our objective is generalizable across various vision models in spite of differences in terms of architectures, regularizers, underlying tasks, etc.

3 PROPOSED APPROACH

In this section, we discuss the proposed data-free objective to craft UAPs in detail.

First, we introduce the notation followed throughout the paper. \mathcal{X} denotes the distribution of images in \mathbb{R}^d . f denotes the function learned by the CNN that maps an input image $x \sim \mathcal{X}$ to its output $f(x)$. Note that the output is task dependent, for example, it is a label for object recognition and segmentation map for semantic segmentation. δ denotes the image-agnostic perturbation learned by our objective. Note that similar to input x , δ also belongs to \mathbb{R}^d . Though the proposed objective is task independent, for ease of understanding we explain the proposed approach in the context of object recognition.

3.1 Data-free objective for fooling

The objective of our paper is to craft an image-agnostic perturbation $\delta \in \mathbb{R}^d$ that fools the CNN f for images from the target distribution \mathcal{X} without utilizing any samples from it. In other words, we seek a universal adversarial perturbation δ that significantly alters the prediction of the CNN (f). That is, we synthesize a δ such that

$$f(x + \delta) \neq f(x), \quad \text{for } x \sim \mathcal{X}. \quad (1)$$

In order for the δ to be an adversarial perturbation, it has to be imperceptible when added to the images. Therefore the pixel intensities of δ are restricted by an imperceptibility constraint. Typically, it is realized as a max-norm constraint in terms l_∞ or l_2 norms (e.g. [5], [8], [9], [11]). In this paper, for all our analysis we impose max-norm constraint in terms of l_∞ norm. Thus, the aim is to find a δ such that

$$\begin{aligned} f(x + \delta) &\neq f(x), \quad \text{for } x \in \mathcal{X}; \\ \|\delta\|_\infty &< \xi. \end{aligned} \quad (2)$$

However, the focus of the proposed work is to craft the image-agnostic perturbations without requiring any data samples (not only from the training dataset \mathcal{X} on which the target model f is learned). The data-free nature of our approach prohibits us from optimizing for the first part of eqn. 2 while learning δ . That is, our approach does not contain the data term x in the proposed objective. Therefore, we propose to fool the CNN by contaminating the extracted representations of the input at multiple layers of the architecture. In other words, as opposed to the typical ‘‘flipping the label’’ objective, we attempt to over-fire the

features extracted at multiple layers. That is, we craft a perturbation δ such that it leads to additional activation firing at each layer and thereby misleading the features (filters) at the following layer. The accumulated effect of the contamination eventually leads the CNN to misclassify the input.

The perturbation essentially causes filters at a particular layer to spuriously fire and abstract out inefficient information. Note that in the presence of data (during attack), in order to mislead the activations from retaining useful discriminative information, the perturbation (δ) has to be highly effective. Also, the imperceptibility constraint (second part of eqn. 2) on δ makes it more challenging.

Hence without utilizing any data (x), we seek for an image-agnostic perturbation δ that can produce maximal spurious activations at each layer of a given CNN. In order to craft such a δ we start with a random perturbation and optimize for the following objective

$$Loss = -\log \left(\prod_{i=1}^K \|l_i(\delta)\|_2 \right), \quad \text{such that } \|\delta\|_\infty < \xi. \quad (3)$$

where $l_i(\delta)$ is the activation in the output tensor at layer i when δ is fed to the network f . Note that the activations are considered after the non-linearity (typically ReLU). K is the total number of layers in f at which we maximize the activations caused by perturbation δ , and ξ is the max-norm limit on δ .

The proposed objective computes product of activation magnitude at all the individual layers in order to simultaneously maximize the interference at all layers. We observed product resulting in stronger δ than other forms of combining (e.g. sum) individual layer activations. This is understandable, since product can force the individual activations to rise in order for the loss to reduce. To avoid working with extreme values (≈ 0), we apply log on the product. Note that the objective is open-ended as there is no optimum value to reach. We would ideally want δ to cause as much strong disturbance at all the layers as possible, while respecting the imperceptibility constraint.

3.2 Implementation Details

We begin with a target network f which is a trained CNN whose parameters are frozen and a random perturbation δ . We then perform the proposed optimization to update δ for causing strong activations at multiple layers in the given network. We typically consider all the convolution (*conv*) layers before the fully connected (*fc*) layers. This is because, the *conv* layers are generally considered to learn required features to extract information over which a series of *fc* layers perform classification. Also, we empirically found that it is efficient to optimize at *conv* layers. Therefore, we restrict the optimization to feature extraction layers. In case of advanced architectures such as GoogLeNet [24] and ResNet [25], we optimize at the last layers of all the inception blocks (or residual blocks) and the independent *conv* layers. We observed that optimizing at these layers results in δ with a fooling capacity similar to the one resulting from optimizing at all layers (including the *conv* layers within the inception/residual blocks). However, since optimizing

at only the last layers of inception/residual blocks along with independent *conv* layers is slightly more efficient, we perform the same.

Note that the optimization updates only the perturbation δ , not the network parameters. Additionally, no image data is involved in the optimization process. We update δ with the gradients computed for loss in eqn. (3) iteratively till the fooling performance of the learned δ gets saturated on a set of validation images. In order to validate the fooling performance of the learned δ , we compose an unrelated substitute dataset (D). Since our objective is not to utilize data samples from the training dataset of the target models, we randomly select 1000 images from a substitute dataset to serve as validation images. Note that, it is a reasonable assumption for an attacker to have access to 1000 unrelated images. For crafting perturbations to object recognition models trained on ILSVRC dataset [26], we choose samples from Pascal VOC-2012 [27] dataset. Similarly, for semantic segmentation models trained on Pascal VOC [27], [28], we choose validation samples from ILSVRC [26], for depth estimation models trained on KITTI dataset [29] we choose samples from Places-205 [30] dataset.

3.3 Exploiting additional priors

Though the proposed method is a data-free optimization for crafting image-agnostic perturbations, it can exploit simple additional priors about the data distribution \mathcal{X} . In this section we demonstrate how our method can utilize simple priors such as (i) mean value and dynamic range of the input, and (ii) target data samples.

3.3.1 Mean and dynamic range of the input

Note that the proposed optimization (eqn. (3)) does not consider any information about \mathcal{X} . We present only the norm limited δ as input and maximize the resulting activations. That is, during the optimization, input to the target CNN has a dynamic range of $[-10, 10]$. However, during the inference time, input lies in $[0, 255]$ range. Therefore, it becomes very challenging to learn perturbations that can affect the neuron activations in the presence of strong (approximately, an order higher) input signal x . Hence, in order to make the learning easier, we provide this useful information about the data ($x \in \mathcal{X}$), and let the optimization better explore the space of perturbations. Thus, we slightly modify our objective to craft δ relative to the dynamic range of the data. We create pseudo data d via randomly sampling from a Gaussian distribution whose mean (μ) is equal to the mean of training data and variance (σ) that covers 99.9% of density to lie in $[0, 255]$, the dynamic range of input. Essentially, we solve for the following

$$Loss = -\log \left(\prod_{i=1}^K \|l_i(d + \delta)\|_2 \right), \quad (4)$$

such that $\|\delta\|_\infty < \xi$, and $d \sim \mathcal{N}(\mu, \sigma)$.

Essentially, we operate the proposed optimization in a closer subspace to the target data distribution \mathcal{X} . In other words, d in eqn. (4) acts as a place holder for the actual data and helps to learn perturbations which can over-fire the neuron activations in the presence of the actual data. For

each iteration of the optimization process, we sample a new d from the normal distribution and feed it through the target CNN. We also perform typical augmentations such as flipping, cropping and slight rotation, etc. on the sampled d to construct variations.

3.3.2 Target data samples

In this subsection, we formulate our data-free objective to utilize samples from the target distribution \mathcal{X} and benefit to improve the fooling ability of the crafted perturbations. Note that in the case of data availability, we can design direct objectives such as reducing confidence for the predicted label or changing the predicted label, etc. However, we investigate if our data-free objective of over-firing the activations, though is not designed to utilize data, crafts better perturbations when data is presented to the optimization. Additionally, our objective does not utilize data to manipulate the predicted confidences or labels. Rather, the optimization benefits from prior information about the data distribution such as the dynamic range, local patterns, etc., which can be provided through the actual data samples. Therefore, with minimal data samples we solve for the following optimization problem

$$Loss = -\log \left(\prod_{i=1}^K \|l_i(x + \delta)\|_2 \right), \quad (5)$$

such that $\|\delta\|_\infty < \xi$, and $x \sim \mathcal{X}$.

Note that presenting data samples to the optimization procedure is a natural extension to presenting the dynamic range of the target data alone (section 3.3.1). In this case, we utilize a subset of training images on which the target CNN models are trained (similar to [8], [11]).

3.4 Improved Optimization

In this subsection, we present the improvements we propose to our earlier optimization presented in our conference paper [9]. The proposed objective in [9] is observed to quickly accumulate δ beyond the imposed max-norm constraint (ξ). Because of the clipping performed after each iteration, the updates will be futile after δ reaching the constraint. In order to tackle this saturation, δ is re-scaled to half of its dynamic range (i.e. $[-5, 5]$) in regular time intervals of 300 iterations. Though this re-scaling helps to learn better δ , it is inefficient since it performs blind re-scaling without verifying the scope for updating the δ . For example, as the learning progresses, magnitude of updates decreases and during the interval of 300 iterations, the values of δ might not reach the extreme values of ± 10 . Projecting the δ by re-scaling can badly affect the learning.

Therefore, we propose an adaptive re-scaling of δ based on the rate of saturation (reaching the extreme values of ± 10) in its pixel values. During the optimization, at each iteration we compute the proportion (p) of the pixels in δ that reached the max-norm limit ξ . As the learning progresses, since our objective is open ended, more number of pixels reach the max-norm limit and because of the clipping eventually get saturated at ξ . Hence, the rate of increase in p decreases as δ saturates. We compute the rate of saturation, denoted as S , of the pixels in δ after each iteration during

the training. For consecutive iterations, if increase in p is not significant (less than a pre-defined threshold Th), we perform a re-scaling to half the dynamic range. Note that the proposed criterion for re-scaling is similar to the typical usage of validation performance to stop training. We observe that the proposed adaptive re-scaling consistently leads to better learning.

3.5 Algorithmic summarization

In this subsection, for the sake of brevity we summarize the proposed data-free objective in the form of an algorithm. Algorithm 1 presents the proposed optimization as a series of steps. Note that it is a generic form comprising of all the three variations including both data-free and with prior versions.

For ease of reference, we repeat some of the notation. F_t is the fooling rate at iteration t , $l_i(x)$ is the activation caused at layer i of the CNN f for an input x , η is the learning rate used for training, Δ is the gradient of the loss with respect to the input δ , S_t is the rate of saturation of pixels in the perturbation δ at iteration t , Th is the threshold on the rate of saturation, F_t is the fooling rate, H is the patience interval of validation for verifying the convergence of the proposed optimization.

Algorithm 1: Algorithm summarizing our approach to craft image-agnostic adversarial perturbations via data-free objective and exploiting various data priors.

Data: Target CNN f , data g . Note that $g = 0$ for data-free case, $g = d \sim \mathcal{N}(\mu, \sigma)$ for range prior case, and $g = x$ for training data samples case.

Result: Image-agnostic adversarial perturbation δ .

```

1 Randomly initialize  $\delta_0 \sim \mathcal{U}[-\xi, \xi]$ 
2  $t = 0$ 
3  $F_t = 0$ 
4 do
5    $t \leftarrow t + 1$ 
6   Compute  $l_i(g + \delta)$ 
7   Compute the loss  $= -\log \left( \prod_{i=1}^K \|l_i(g + \delta)\|_2 \right)$ 
8   Update1  $\delta_t : \delta_t \leftarrow \delta_{t-1} - \eta \Delta$ 
9   Compute the rate of saturation  $S_t$  in the  $\delta_t$  pixels
10  if  $S_t < Th$  then
11     $\delta_t \leftarrow \delta_t / 2$ 
12  end
13  Compute  $F_t$  of  $\delta_t$  on substitute dataset  $D$ 
14 while  $F_t < \min. \text{ of } \{F_{t-H}, F_{t-H+1} \dots F_{t-1}\}$ ;
15  $i \leftarrow \text{argmax. of } \{F_{t-H}, F_{t-H+1} \dots F_{t-1}\}$ 
16 Return  $\delta_i$ 

```

¹Note that this generic update equation is only for understanding purpose and not the exact equation implemented.

3.6 Generalized Fooling Rate (GFR) with respect to a metric

While the notion of ‘fooling’ has been well defined for the task of image recognition, for other tasks, how to measure the ‘fooling’ is unclear. Hence, in order to provide an interpretable metric to measure ‘fooling’, we introduce

Generalized Fooling Rate (GFR), making it independent of the task, and dependent on the metric being used for evaluating the model’s performance.

Consider the task of image recognition. For this task, fooling rate for any perturbation is defined as the % of data samples, for which the labels are changed due to the perturbation. i.e., the % of data samples for which the output label before and after the adversarial attack are different. If the fooling rate is $x\%$, then for $(100 - x)\%$ of the data samples, the label before and after the adversarial attack remains the same. If we consider the labels of clean samples as ground truth, and labels of perturbed samples as predicted labels, $(100 - x)\%$ is same as the Top-1 accuracy of the model. This leads us to introduce the following definition for the Generalized Fooling Rate.

Let M be a metric for measuring the performance of a model for any task, where the range of M is $[0, R]$. Let the metric take two inputs \hat{y} and y , where \hat{y} is the predicted output and y is the ground truth output, such that the performance of the model is measured as $M(\hat{y}, y)$. Let \hat{y}_δ be the output of the model when the input is perturbed with a perturbation δ . Then, the Generalized Fooling Rate with respect to measure M is defined as:

$$GFR(M) = \frac{R - M(\hat{y}_\delta, \hat{y})}{R}. \quad (6)$$

This definition of Generalized Fooling rate (GFR) has the following benefits:

- Fooling rate should be a measure of the change in model’s output caused by the perturbation. Being independent of the ground truth y , and dependant only on \hat{y}_δ and \hat{y} , GFR primarily measures the change in the output. Other methods such as the metric value after the attack may not properly capture this. A poorly performing model which however is very robust to adversarial attacks will show very poor GFR values, highlighting its robustness. For example, GFR will be equal to 0% if there is no change in the output, and in extreme cases it can reach 100%, for a given task. Hence it can be compared across tasks.
- GFR measures the performance of a perturbation in terms of the damage caused to a model with respect to a metric. This is an important feature, as tasks such as depth estimation have multiple performance measures, where some perturbation might cause harm only to some of the metrics while leaving other metrics unaffected.

For all the tasks considered in this work, we report GFR with respect to a metric, as a measure of ‘fooling’.

4 EXPERIMENTS

In this section, we present the experimental evaluation to demonstrate the effectiveness of the proposed data-free objective. We consider three different vision tasks to demonstrate the generalizability of our objective, namely, object recognition, semantic segmentation and unsupervised monocular depth estimation. Note that the set of applications include both classification and regression tasks. Also, it has both supervised and unsupervised learning setups.

TABLE 1

Fooling rates for the proposed data-free objective learned for object recognition on ILSVRC dataset [26]. Each row of the table shows the fooling rates for the perturbation learned on a specific target model when attacking various other models (columns). These rates are obtained by the proposed objective without utilizing the data samples but only the range prior (sec. 3.3.1). Diagonal rates indicate the white-box attack scenario and off-diagonal ones represent the black-box attack scenario. Note that the highest fooling rate when attacking a given model (column) is shown in bold.

Model	CaffeNet	VGG-F	GoogLeNet	VGG-16	VGG-19	Resnet-152
CaffeNet	87.02	65.97	49.40	50.46	49.92	38.57
VGG-F	59.89	91.91	52.24	51.65	50.63	40.72
GoogLeNet	44.70	46.09	71.44	37.95	37.90	34.56
VGG-16	50.05	55.66	46.59	63.08	56.04	36.84
VGG-19	49.11	53.45	40.90	55.73	64.67	35.81
Resnet-152	38.41	37.20	33.22	27.76	26.52	37.3

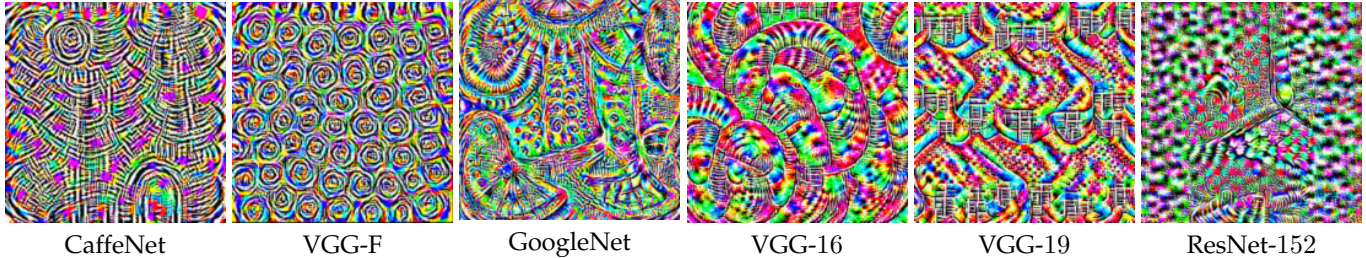


Fig. 1. Universal adversarial perturbations crafted by the proposed data-free objective for multiple models trained on ILSVRC [26] dataset. Perturbations were crafted with $\xi = 10$ using the minimal prior, i.e. mean and dynamic range of the input samples (sec. 3.3.1). Corresponding target network architecture is mentioned below each perturbation. Images are best viewed in color.

We explain each of the tasks separately in the following subsections.

For all the experiments, the ADAM [31] optimization algorithm is used with the learning rate of 0.1. The threshold Th for the rate of saturation S is set to 10^{-5} . Validation fooling rate F_t is measured on the substitute dataset D after every 200 iterations only when the threshold of the rate of saturation is crossed. If it is not crossed, F_t is still measured after every 400 iterations. Note that none of the algorithm specific hyper-parameters are changed across tasks or across prior scenarios.

4.1 Object recognition

We have worked with models trained on ILSVRC [26] and Places-205 [30] datasets, viz. CaffeNet [32], VGG-F [33], GoogLeNet [24], VGG-16 [34], VGG-19 [34], ResNet-152 [25]. Since our approach does not involve training the models, for all the experiments we work with available trained models. Also, unlike UAP [8], as we do not use training data in the data-free case (sec. 3.1 and sec. 3.3.1), no training data is used. However, as explained earlier, we use 1000 images randomly chosen from Pascal VOC-2012 [27] train images as validation set (D in Algorithm 1) for our optimization. Also, in case of exploiting additional data prior (sec. 3.3.2), we use limited data from the corresponding training set. However, for evaluating the perturbations learned for the target models trained on ILSVRC dataset, 50000 images from the validation set are used. Similarly, Places-205 dataset contains 20500 validation images from 205 categories, over which the fooling rates are computed.

4.1.1 Fooling performance of the data-free objective

Table 1 presents the fooling rates achieved by our objective on various network architectures. Fooling rate is the per-

centage of test images for which our crafted perturbation δ successfully changed the predicted label. Higher the fooling rate, greater is the perturbation’s ability to fool and lesser is the classifier’s robustness. Fooling rates in Table 1 are obtained using the mean and dynamic range prior of the training distribution (sec. 3.3.1). Each row in the table indicates one target model employed in the learning process and the columns indicate various models attacked using the learned perturbations. The diagonal fooling rates indicate the *white-box attacking*, where all the information about the model is known to the attacker. The off-diagonal rates indicate *black-box attacking*, where no information about the model under attack is revealed to the attacker. However, note that the dataset over which both the models (target CNN and the CNN under attack) are trained is same. Our perturbations cause a mean white-box fooling rate of 69.24% and a mean black-box fooling rate of 45.13%. Note that, given the data-free nature of the optimization, the fooling rates are alarmingly significant. These high fooling rates achieved by the proposed approach can adversely affect the real-world deployment of these models.

Figure 1 shows example image-agnostic perturbations (δ) crafted by the proposed method. Note that the perturbations look very different for each of the target CNNs. However, the perturbations corresponding to the VGG models look slightly similar owing to their architectural similarity. Figure 3 shows sample perturbed images ($x + \delta$) for VGG-19 [34] from ILSVRC [26] validation set. The top row shows the clean and bottom row shows the corresponding adversarial images. Note that the adversarially perturbed images are visually indistinguishable from their corresponding clean images. All the clean images shown in the figure are correctly classified and are successfully fooled by the added perturbation. Below each image, the corresponding

TABLE 2

Fooling rates achieved by the proposed objective with and without utilizing the prior information about the training distribution of the models. For comparison, we provide the random baseline ($\mathcal{U}[-\xi, \xi]$), existing data-free [9] and data dependent [8] objectives. Note that the best fooling rate for a given model (row) is shown in bold.

Model	Baseline	No prior	Range prior	Data prior	FFF [9]	UAP [8]
CaffeNet	12.9	84.88	87.02	91.54	80.92	93.1
VGG-F	12.62	85.96	91.81	92.64	81.59	93.8
Googlenet	10.29	58.62	71.44	83.54	56.44	78.5
VGG-16	8.62	45.47	63.08	77.77	47.10	77.8
VGG-19	8.40	40.68	64.67	75.51	43.62	80.8
Resnet-152	8.99	29.78	37.3	66.68	-	84.0

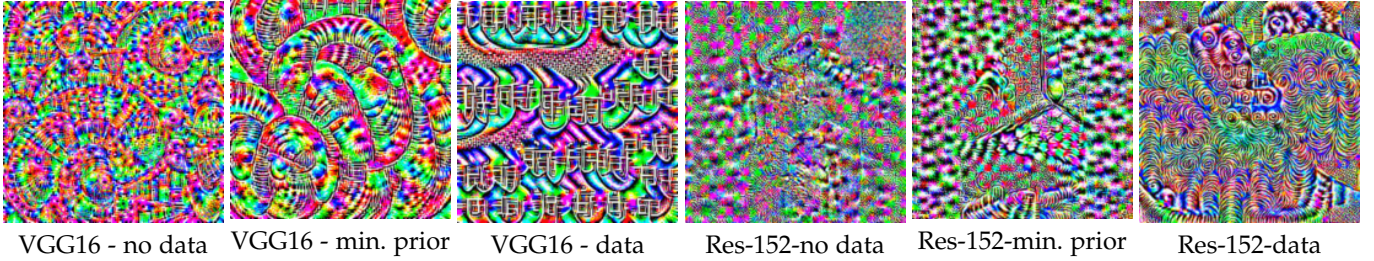


Fig. 2. Sample universal adversarial perturbations crafted by the proposed method under multiple settings for a pair of models trained on ILSVRC [26] dataset. Perturbations were crafted with $\xi = 10$ for no data, minimal data prior and with data scenarios. First three perturbations are crafted for VGG-16 [34] and the later three for ResNet-152 [25]. Corresponding setting is mentioned below each perturbation. Images are best viewed in color.

label predicted by the model is shown. Note that the correct labels are shown in black color and the wrong ones are shown in red.

4.1.2 Exploiting the minimal prior

In this section, we present experimental results to demonstrate how our data-free objective can exploit the additional prior information about the target data distribution as discussed in section 3.3. Note that we consider two cases: (i) providing the mean and dynamic range of the data samples, denoted as range prior (sec. 3.3.1), and (ii) utilizing minimal data samples themselves during the optimization, denoted as data prior (3.3.2).

Table 2 shows the fooling rates obtained with and without utilizing the prior information. Note that all the fooling rates are computed for white-box attacking scenario. To emphasize the effectiveness of the proposed objective, we present fooling rates obtained by a random baseline perturbation. Since our learned perturbation is norm limited by ξ , we sample random δ from $\mathcal{U}[-\xi, \xi]$ and compute the fooling rates. We denote these results in the ‘Baseline’ column of Table 2. Also, for comparison, fooling rates obtained by our data-free objective [9] and a data dependent objective [8] are presented. Important observations to draw from the table are listed below:

- Utilizing the prior information consistently improves the fooling ability of the crafted perturbations.
- A simple range prior can boost the fooling rates on an average by an absolute 10%.
- Given the proposed objective is not designed to utilize the data, feeding the data samples results in an absolute 22% rise in the fooling rates. For some of the models (e.g. GoogLeNet and VGG-16) our method performs equally (or even outperforms) to

TABLE 3

Comparison of data-free objectives. Fooling rates achieved by the proposed objective of maximizing the l_2 norm of the activations caused by δ versus the mean activation [9] when utilizing data samples. Note that the proposed objective consistently outperforms the previous objective across multiple architectures (shown in bold).

Model	Mean activation [9]	l_2 norm
CaffeNet	88.35	91.54
VGG-16	72.68	77.77
Resnet-152	65.43	66.68

an objective [8] designed especially to utilize data and flip the predicted labels.

- Our improved objective (eqn.3) and the optimization procedure (3.4) result in an absolute increase of fooling rate by 22.36% in the case of utilizing data.

4.1.3 Comparison of the data-free objectives

In this subsection we compare the effectiveness of the proposed objective against the existing data-free objective proposed in our conference publication [9]. That is, we compare maximizing the mean versus l_2 norm (energy) of the activations caused by the perturbation δ (or $x/d + \delta$ in case of exploiting the additional priors).

Table 3 shows the comparison of fooling rates obtained with both the objectives (separately) in the improved optimization setup (3.4). We have chosen 3 representative models across various generations of architectures (CaffeNet, VGG and ResNet) to compare the effectiveness of the proposed objective. Note that the improved objective consistently outperforms the previous one by a significant 3.18%. Similar behaviour is observed for other vision tasks also.

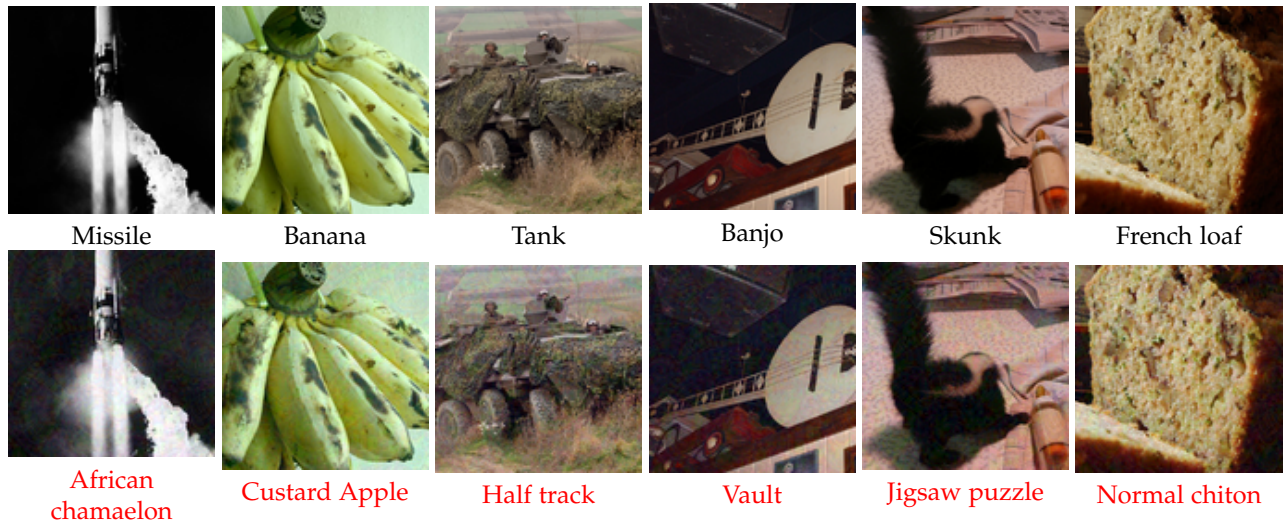


Fig. 3. Sample original and adversarial image pairs from ILSVRC validation set generated for VGG-19. First row shows original images and corresponding predicted labels, second row shows the corresponding perturbed images along with their predictions. Note that all of the shown perturbed images were misclassified.

TABLE 4

Effect of data dependency on crafting the perturbations. Data dependent objectives [8] suffer significant drop in fooling ability when arbitrary data samples are utilized for crafting image-agnostic perturbations. Note that, $A \rightarrow B$ denotes that data A is used to craft perturbations to fool models trained on data B. Also note that fooling rates for our approach are crafted without utilizing any data samples (denoted with *).

Model	Places-205 \rightarrow ILSVRC		ILSVRC \rightarrow Places-205	
	Ours	UAP [8]	Ours	UAP [8]
CaffeNet	87.02*	73.09	88.61*	77.21
GoogLeNet	71.44*	28.17	83.37*	52.53

4.1.4 Data dependent vs. Data-free objectives

In this subsection we demonstrate the necessity of data dependent objective [8] to have samples from the target distribution only. That is, methods (such as [8]) that craft perturbations with fooling objective (i.e. move samples across the classification boundaries) require samples from only the training data distribution during the optimization. We show that crafting with arbitrary data samples leads to significantly inferior fooling performance.

Table 4 shows the fooling rates of data dependent objective [8] when arbitrary data samples are utilized in place of target samples. Experiment in which we use Places-205 data to craft perturbations for models trained on ILSVRC is denoted as Places-205 \rightarrow ILSVRC and vice versa. For both the setups, a set of 10000 training images are used. Note that, the rates for the proposed method are obtained without utilizing any data and rates for data-free scenario can be found in Table 2. Clearly the fooling rates for UAP [8] suffer significantly, as their perturbations are strongly tied to the target data. On the other hand, for the proposed method, since it does not craft via optimizing a fooling objective, the fooling performance does not decrease. Importantly, these experiments show that the data dependent objectives are not effective when samples from the target distribution are not

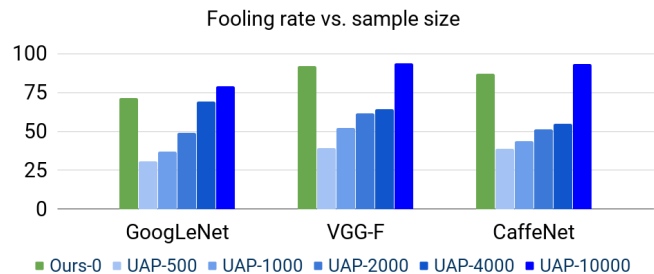


Fig. 4. Reliance of the data dependent objective UAP [8] on the size of available training data samples. Fooling rate of the crafted perturbations monotonically increases with the number of training data samples available during the optimization. Note that our approach utilizes no data samples and achieves competitive fooling performance.

available. In most of the practical scenarios it is difficult to procure the same training data. Also, as the data dependent objectives rely on the available training data, the ability of the crafted perturbations heavily depends on the size of the data utilized in the crafting process. We show that the fooling performance of UAP [8] monotonically increases with the size of the available samples for optimization. Figure 4 shows the fooling rates obtained by the perturbations crafted for multiple recognition models trained on ILSVRC by UAP [8] with varying size of samples available for optimization. We craft different UAP [8] perturbations (using the codes provided by the authors) utilizing only 500, 1000, 2000, 4000 and 10000 data samples and evaluate their ability to fool various models. Note that the performance of the crafted perturbations increases drastically (shown in different shades of blue) with the available data samples during the optimization. For comparison, the fooling rates obtained by the proposed data-free objective is shown in green.

TABLE 5

Comparison of mean IOU obtained by various models against the proposed perturbations. Comparison with image specific adversaries [20] is also presented. Note that * denotes being image-specific and † denotes a transfer attack (black-box attacking). Note that being image specific, [20] outperforms our perturbations, however, even our no data perturbations cause more drop in mIOU than their transfer perturbations.

Model	Original	Baseline	No Data	Range prior	All data	Data w/ less BG	ICCV 2017 [20]
FCN-Alex	46.21	45.72	15.35	10.37	10.64	8.03	3.98*
FCN-8s-VGG	65.49	64.34	42.78	39.08	33.61	28.05	4.02*
DL-VGG	62.10	61.13	36.91	35.41	44.90	27.41	43.96*†
DL-RN101	74.94	73.42	56.40	58.66	37.45	39.00	73.01*†

TABLE 6

Generalized fooling rates achieved by the perturbations crafted by the proposed approach under various settings. Note that for comparison, fooling rates achieved by random perturbations are also presented.

Model	Baseline	No Data	Range Prior	All Data	Data W/ less BG
FCN-Alex	14.29	80.15	86.57	85.96	89.61
FCN-8s-VGG	9.24	49.42	55.04	61.15	67.19
DL-VGG	10.66	55.90	58.96	44.82	66.68
DL-RN101	8.8	37.06	35.6	58.62	56.61

4.2 Semantic segmentation

In this subsection we demonstrate the effectiveness of our data-free objective to craft universal adversarial perturbations for semantic segmentation. We consider four network architectures. The first two architectures are from FCN [35]: **FCN-Alex**, based on Alexnet [32], and **FCN-8s-VGG**, based on the 16-layer VGGNet [34]. The last two architectures are 16-layer VGGNet based **DL-VGG** [36], and **DL-RN101** [37], which is a multi-scale architecture based on ResNet-101 [25].

The FCN architectures are trained on Pascal VOC-2011 dataset [28], [38], consisting 9610 training samples and the remaining two architectures are trained on Pascal VOC-2012 dataset [27], [38], consisting 10582 training samples. However, for testing our perturbation’s performance, we only use the validation set provided by [35], which consist of 736 images.

Semantic segmentation is realized as assigning a label to each of the image pixels. That is, these models are typically trained to perform pixel level classification into one of 21 categories (including the background) using the cross-entropy loss. Performance is commonly measured in terms of mean IOU (intersection over union) computed between the predicted map and the ground truth. Extending the UAP generation framework provided in [8] to segmentation is a non-trivial task. However, our generalizable data-free algorithm can be applied for the task of semantic segmentation without any changes.

Similar to recognition setup, we present multiple scenarios for crafting the perturbations ranging from no data to utilizing data samples from the target distribution. An interesting observation with respect to the data samples from Pascal VOC-2012, is that, in the 10582 training samples, 65.4% of the pixels belong to the ‘background’ category. Due to this, when we craft perturbation using training data samples as target distribution prior, our optimization process encounters roughly 65% pixels belonging to

‘background’ category, and only 35% pixels belonging to the rest 20 categories. As a result of this data imbalance, the perturbation is not sufficiently capable to corrupt the features of pixels belonging to the categories other than ‘background’. To handle this issue, we curate a smaller set of 2833 training samples from Pascal VOC-2012, where each sample has less than 50% pixels belonging to ‘background’ category. We denote this as “data with less BG”, and only 33.5% of pixels in this dataset belong to the ‘background’ category. The perturbations crafted using this dataset as target distribution prior show a higher capability to corrupt features of pixels belonging to the rest 20 categories. Since mean IOU is the average of IOU for each of the 21 categories, we further observe that perturbations crafted using “data with less BG” cause a substantial reduction in the mean IOU measure as well.

Table 6 shows the generalized fooling rates with respect to the mean IOU obtained by the proposed objective under various data priors. As explained in section 3.6, the generalized fooling rate measures the change in the performance of a network with respect to a given metric, which in our case is the mean IOU. Note that, similar to the recognition case, the fooling performance monotonically increases with the addition of data priors. This observation emphasizes that the proposed objective, though being an indirect and non-fooling in nature, can rightly exploit the additional prior information about the training data distribution. Also, of all the models, generally, data with less background scenario results in the best fooling rate. This can be attributed to the fact that in data with less background scenario we lessen the data-imbalance that leads to perturbations that can fool both background and object pixels. Also, for comparison, we present the fooling rates achieved by the random perturbation sampled from $\mathcal{U}[-\xi, \xi]$. Note that similar to recognition experiments, for all the segmentation experiments we use a ξ value of 10.

In Table 5 we present the mean IOU metric obtained on the perturbed images learned under various scenarios along with original mean IOU obtained on clean images. Comparison with baseline random noise perturbation sampled from $\mathcal{U}[-10, 10]$ is also provided. It is clearly observed that the random perturbation is not effective in fooling the segmentation models. However, the proposed objective crafts perturbations within the same range that can significantly fool the models. We also show the mean IOU obtained by Xie *et al.* [20], an image specific adversarial perturbation crafting work. Note that since the proposed method is an image-agnostic approach it is unfair to expect

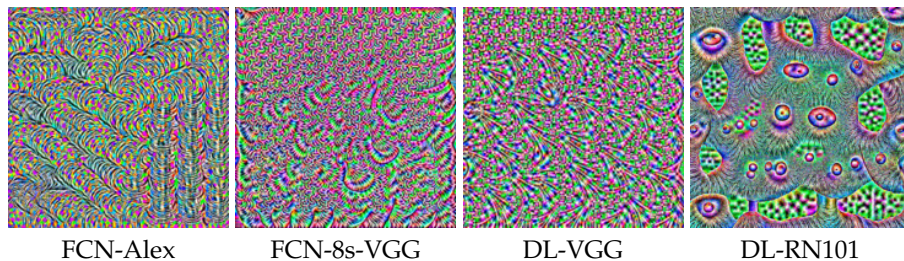


Fig. 5. Universal adversarial perturbations for semantic segmentation, crafted by the proposed data-free objective for multiple models. Perturbations were crafted with $\xi = 10$ using the less BG prior. Corresponding target network architecture is mentioned below each perturbation. Images are best viewed in color.

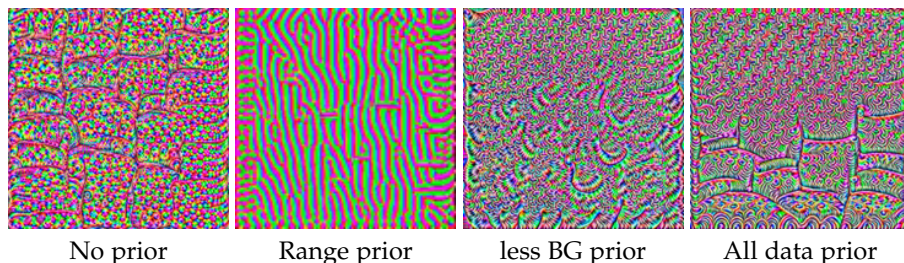


Fig. 6. Sample universal adversarial perturbations for semantic segmentation, crafted by the proposed method under multiple settings for **FCN-8s-VGG**. Perturbations were crafted with $\xi = 10$ for no prior, range prior, data with less BG prior, and all data prior scenarios. Corresponding scenario is mentioned below each perturbation. Images are best viewed in color.

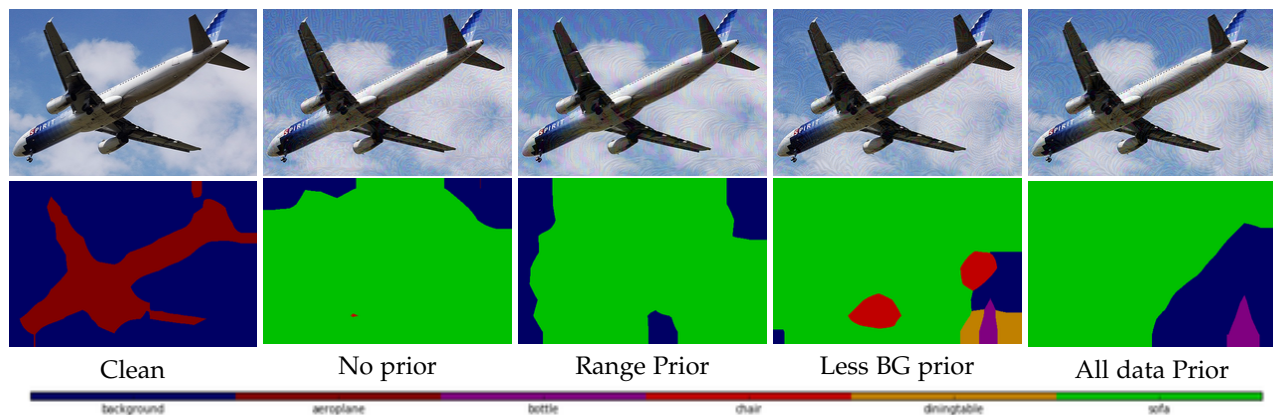


Fig. 7. Sample original and adversarial images from PASCAL-2011 dataset generated for **FCN-Alex**. First row shows clean and adversarial images with various priors. Second row shows the corresponding predicted segmentation maps.

similar performance as [20]. Further, the mean IOU shown by [20] for **DL-VGG** and **DL-RN101** models (bottom 2 rows of Table 5) denote the transfer performance, i.e., black-box attacking and hence the smaller drop of the mean IOU from that of clean images. However, they are provided as a means of weak comparison instead of no comparison.

Finally, we end this section by providing some qualitative results. Figure 5 and 6 shows sample image-agnostic adversarial perturbations learned by our objective for semantic segmentation. In Figure 5 we show the perturbations learned with “data with less BG” prior for all the models. Similar to the recognition case, these perturbations look different across architectures. In Figure 6, we show the perturbations learned for **FCN-8s-VGG** model under various scenarios ranging from no prior to full data prior. Note that, even for a given network, the perturbations learned with various priors look different. Figures 7 shows example

image and predicted segmentation outputs by **FCN-Alex** model for perturbations crafted with various priors. Top row shows the clean and the perturbed images. Bottom row shows the predictions for the corresponding inputs. Note that the type of prior utilized to craft the perturbation is mention below the predictions. Crafted perturbations are clearly successful in misleading the model to predict inaccurate segmentation maps. Note that the color map shown below the predictions provides the labels.

Figure 8 shows the effect of perturbation on multiple networks. It shows the output maps predicted by various models for the same input perturbed with corresponding δ learned with “data with less BG” prior. It is interesting to note from Figure 8 that for the same image, with UAPs crafted using the same prior, different networks can have very different outputs, even if their outputs for clean images are very similar.

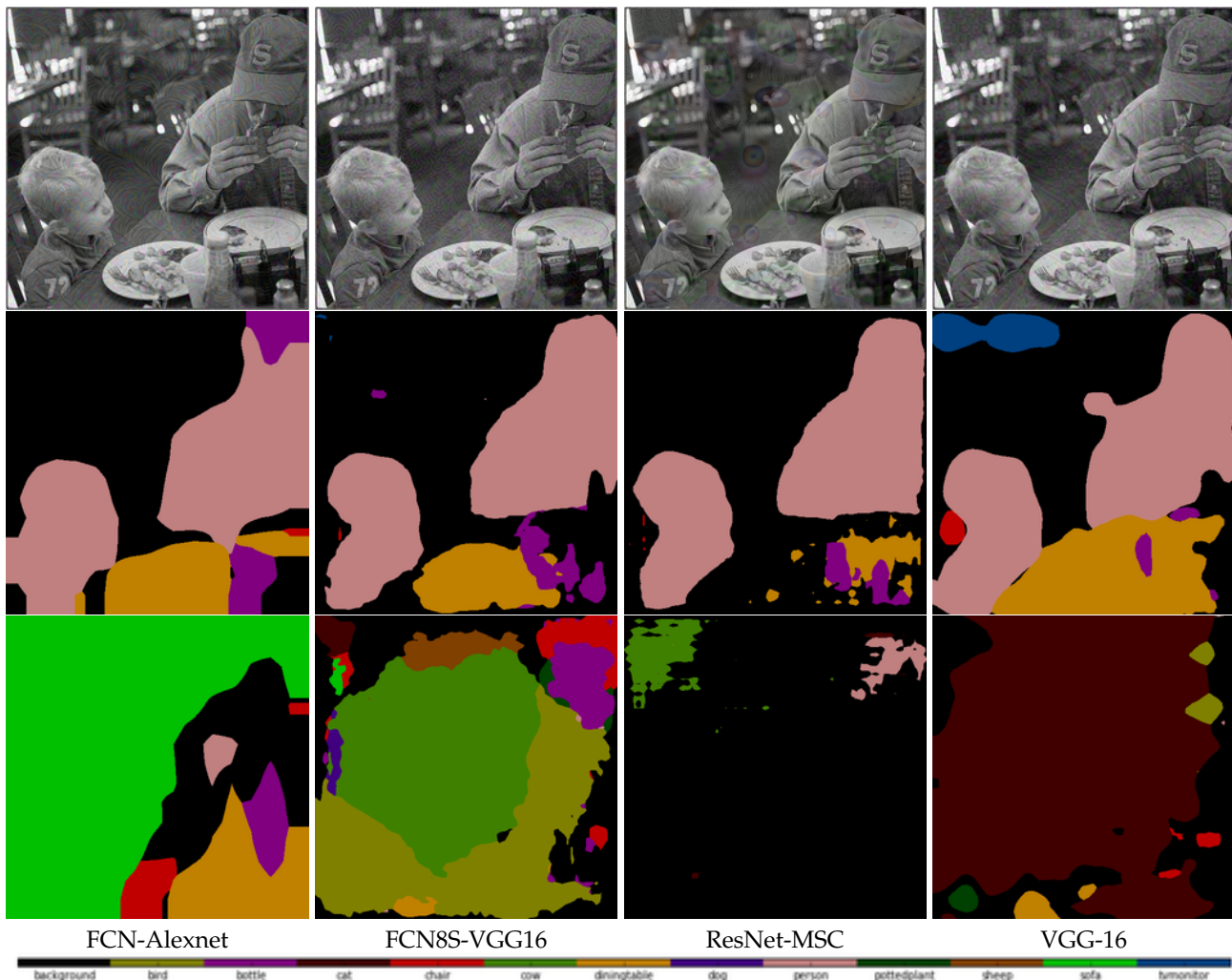


Fig. 8. Segmentation predictions of multiple models over a sample perturbed image. Perturbations were crafted with $\xi = 10$ using the “data with less BG” prior. The first row shows the perturbed input image, the second shows the segmentation output of clean sample image, and the third shows the segmentation output of the perturbed sample image. The corresponding target network architecture is mentioned below each column. Images are best viewed in color.

4.3 Depth estimation

Recent works such as [39], [40], [41] show an increase in use of convolutional networks for regression-based Computer Vision task. A natural question to ask is whether they are as susceptible to universal adversarial attacks, as CNNs used for classification. In this section, by crafting UAPs for convolutional networks performing regression, we show that they are equally susceptible to universal adversarial attacks. To the best of our knowledge, we are the first to provide an algorithm for crafting universal adversarial attacks for convolutional networks performing regression.

Many recent works like [39], [42], [43] perform depth estimation using convolutional network. In [39], the authors introduce Monodepth, an encoder-decoder architecture which regresses the depth of given monocular input image. We craft UAP using the proposed method for the two variants of Monodepth, **Monodepth-VGG** and **Monodepth-Resnet50**. The network is trained using KITTI dataset [29]. In its raw form, the dataset contains 42,382 rectified stereo pairs from 61 scenes, with a typical image being 1242×375 pixels in size. We show results on the eigen

split, introduced in [44], which consist of 23488 images for training and validation, and 697 images for test. We use the same crop size as suggested by the authors of [44] and evaluate at the input image resolution.

As in the case of object recognition, UAPs crafted by the proposed method for monodepth also show the potential to exploit priors about the data distribution. We consider three cases, (i) providing no priors, (ii) range prior, and (ii) data prior. For providing data priors, we randomly pick 10000 image samples from the KITTI train dataset. To attain complete independence of target data in the training procedure, while crafting the perturbation, we perform validation on a set of 1000 randomly picked images from Places-205 dataset. The optimization procedure followed is the same as in the case of the previous two task.

Table 7 and 8 show the performance of **Monodepth-Resnet50**, and **Monodepth-VGG** respectively under the presence of the various UAPs crafted by the proposed method. As can be observed from the tables, the crafted UAPs have a strong impact on the performance of the networks. For both the variants of monodepth, UAPs crafted

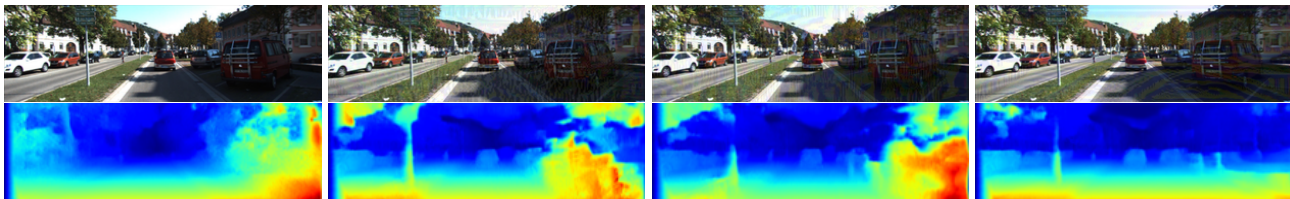


Fig. 9. Sample original and adversarial image pairs from KITTI dataset generated for **Monodepth-VGG**. First row shows clean and perturbed images with various priors. Second row shows the corresponding predicted depth maps.

TABLE 7

Performance of the crafted perturbations for **Monodepth-Resnet50** using various metrics for evaluating depth estimation on the eigen test-split of KITTI dataset. Results are presented for various scenarios such as clean data (Normal), perturbations learned with no prior, various priors and the train set mean. Note that the best fooling results for each scenario are shown in bold. The evaluation of trainset mean performance has been taken from [45]. Note that the first four metrics are error based (higher means better fooling, indicated as \uparrow) and the later three are precision based (lower is better fooling, indicated as \downarrow).

Perturbation	Abs Rel (\uparrow)	Sq Rel (\uparrow)	RMSE (\uparrow)	RMSE log (\uparrow)	$\delta < 1.25$ (\downarrow)	$\delta < 1.25^2$ (\downarrow)	$\delta < 1.25^3$ (\downarrow)
Normal	0.133	1.148	5.549	0.230	0.829	0.935	0.970
Baseline	0.1339	1.1591	5.576	0.231	0.827	0.934	0.969
No prior	0.201	1.810	6.603	0.352	0.688	0.840	0.908
Range prior	0.319	3.292	9.064	0.640	0.460	0.611	0.717
Data prior	0.380	10.278	10.976	0.402	0.708	0.842	0.900
Train set mean	0.361	4.826	8.102	0.377	0.638	0.804	0.894

TABLE 8

Performance of the crafted perturbations for **Monodepth-VGG** using various metrics for evaluating depth estimation on the eigen test-split of KITTI dataset. Results are presented for various scenarios such as clean data (Normal), perturbations learned with no prior, various priors and the train set mean. Note that the best fooling results for each scenario are shown in bold. The evaluation of trainset mean performance has been taken from [45]. Note that the first four metrics are error based (higher means better fooling, indicated as \uparrow) and the later three are precision based (lower is better fooling, indicated as \downarrow).

Perturbation	Abs Rel (\uparrow)	Sq Rel (\uparrow)	RMSE (\uparrow)	RMSE log (\uparrow)	$\delta < 1.25$ (\downarrow)	$\delta < 1.25^2$ (\downarrow)	$\delta < 1.25^3$ (\downarrow)
Normal	0.148	1.344	5.927	0.247	0.803	0.922	0.964
Baseline	0.149	1.353	5.949	0.248	0.800	0.920	0.963
No prior	0.192	1.802	6.626	0.325	0.704	0.861	0.929
Range prior	0.212	2.073	6.994	0.364	0.658	0.825	0.906
Data prior	0.355	9.612	10.592	0.390	0.714	0.850	0.908
Train set mean	0.361	4.826	8.102	0.377	0.638	0.804	0.894

with range prior, bring down the accuracy with the threshold of 1.25 units ($\delta < 1.25$) by 25.7% on an average. With data priors, the crafted UAPs are able to increase the Sq Rel (an error metric) to almost 10 times the original performance. Under the impact of the crafted UAPs, the network’s performance drops below that of the baseline, which uses the train set mean as the prediction for all image pixels.

Table 9 shows the Generalized Fooling Rates with respect to the accuracy with the threshold of 1.25 units ($\delta < 1.25$). A surprising observation from the table is that the performance of the range prior perturbations on both the networks surpasses that of the data prior perturbations. This might lead us to understand that the range prior perturbations are stronger. However the Generalized Fooling Rate (GFR) measures the change in a network’s outcome, with respect to a metric. As observed from Table 7 and 8, the data prior perturbations have a much harsher effect on the error metrics like Root Mean Square Error (RMSE), whereas range prior perturbations have a harsher effect on precision metrics like $\delta < 1.25$. Hence, ‘which perturbation is better?’, is rather a metric dependant question and conclusions based on a

TABLE 9

Generalized Fooling rate with respect to $\delta < 1.25$ metric for the task of depth estimation

Model	Baseline	No data	Range prior	Data prior
Monodepth-VGG	0.4%	15.3%	22.7%	21.3%
Monodepth-Resnet50	2%	21.3%	47.6%	24.3%

single metric would only partially reflect the truth.

Figures 9 and 11 show some qualitative examples, showing the perturbed input and the change in output. Figure 9 shows the input-output pair for **Monodepth-VGG**, where the input is perturbed by the various kinds of UAPs crafted. Figure 11 compares the input-output pair for **Monodepth-VGG** and **Monodepth-Resnet50** using the range-prior UAP. As show by figures 9 and 11, for both versions of Monodepth, quasi-imperceptible change in the input can cause a large change in the output.

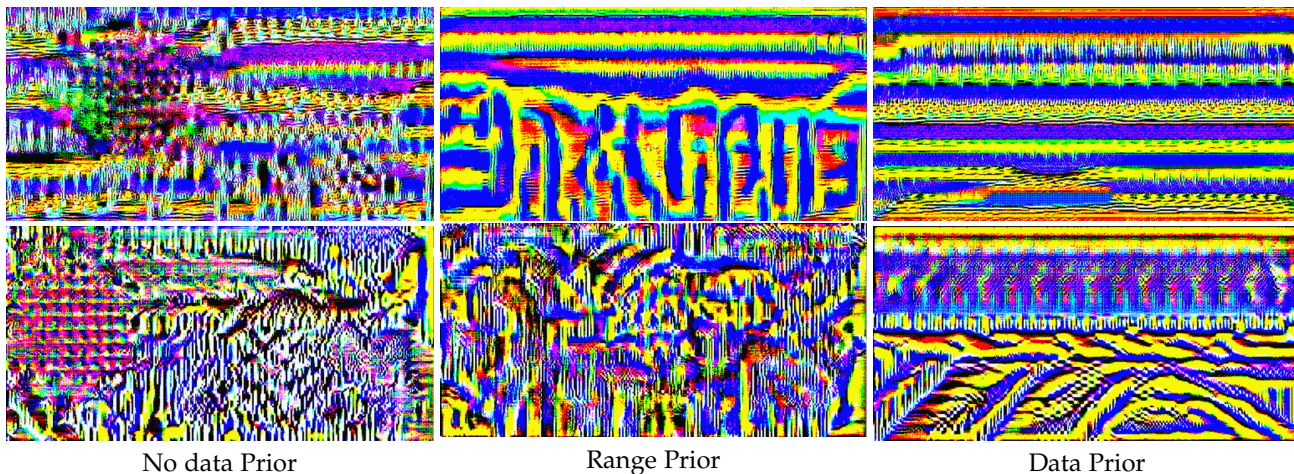


Fig. 10. Universal adversarial perturbations for depth estimation task crafted using our proposed algorithm. Top row shows the perturbations learned for **Monodepth-Resnet50** and the bottom row shows that for **Monodepth-VGG**. Perturbations were crafted with $\xi = 10$ for no prior, range prior, and all data prior scenarios. Corresponding scenario is mentioned below each column. Images are best viewed in color.

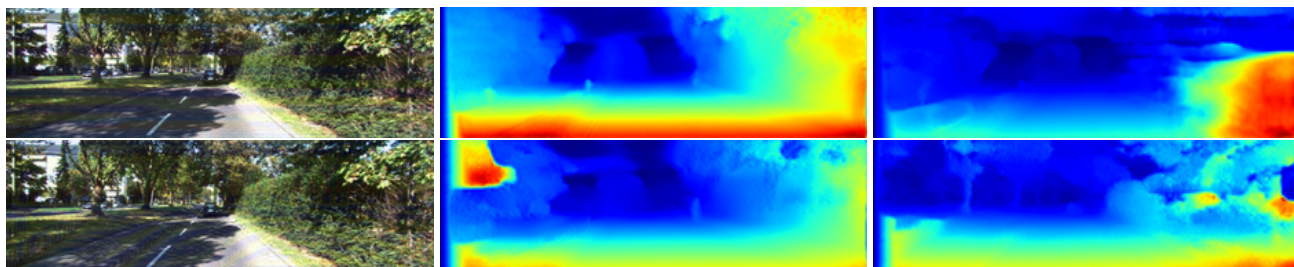


Fig. 11. Depth predictions of both models over a sample perturbed image. Perturbations were crafted with $\xi = 10$ using the range prior. The top row corresponds to **Monodepth-Resnet50** and the bottom row corresponds to **Monodepth-VGG**. The first column shows the perturbed input image, the second shows the depth output of clean sample image, and the third shows the depth output of the perturbed sample image. Images are best viewed in color.

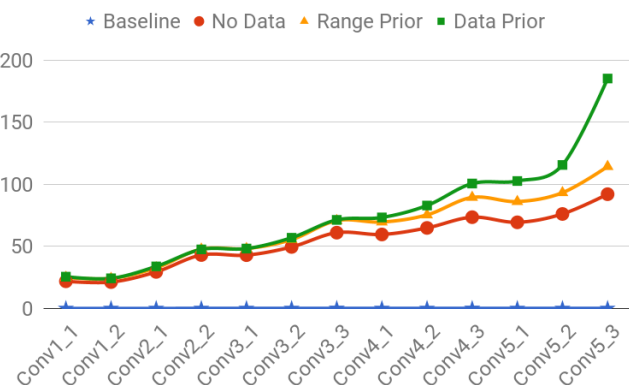


Fig. 12. Percentage relative change in the extracted representations caused by our crafted perturbations at multiple layers of VGG-16. Note that as we do deeper into the net, the amount of perturbation increases drastically which results in eventual misclassification of the input.

5 DISCUSSION

As demonstrated by our experimentation in section 4, it is evident that the proposed algorithm is able to craft perturbations which achieve ‘fooling’ for a variety of computer vision tasks. An important question to ask about the Convolutional neural Networks (CNNs), is “How stable are

the learned representations at each layer?” That is, Are the features learned by the CNNs robust to small changes in the input? or Can a small change in the input layer leads to a huge change in its output? As mentioned earlier ‘fooling’ refers to instability of the CNN in terms of its output, independent of the task at hand.

Earlier works (e.g., [4], [5], [8]) have proven that the CNNs can be fooled by small but learned noise. Most of these works (e.g., [5]) rely on data to find these directions in which the input can be slightly perturbed in order to fool the CNN. These approaches try to find via simple methods such as gradient ascent, the directions in which the network’s confidence falls. Recent works by Moosavi-Dezfooli *et al.* [7], [8] find the nearest classification boundary for a given sample and perturb it by moving across the boundary thereby achieve the fooling. They also establish that it is possible to learn a single perturbation which can work for most of the input images. Thus existing works (independent of the underlying task) exploit data samples, model’s confidence and the classification boundaries in the input space in order to craft the adversarial perturbations, either image specific or agnostic.

Unlike the existing works, we depict this as a stability issue with the learned representations by CNNs. We attempt to learn the optimal perturbation in the input space that can cause maximal change in the output of the network.

TABLE 10

Relative Shift in Classification Layer’s input and the fooling rate, for **VGG-16** in the task of classification. The relative shift has been evaluation on 1000 random images from ILSVRC validation set, while the fooling rate is evaluated on the entire ILSVRC validation set.

Perturbation	Rel. Shift in input to f_{c_8} (classification) layer	Fooling rate
Baseline	0.0006	8.62
No Prior	0.867	45.47
Range Prior	1.142	63.08
All data Prior	3.169	77.77

We achieve this via learning perturbations that can result in maximal change in the activations at all the intermediate layers of the architecture. As an example, we consider VGG-16 CNN trained for object recognition to illustrate the working of our objective. Figure 12 shows the percentage relative change in the feature activations ($\frac{\|l_i(x+\delta)-l_i(x)\|_2 \times 100}{\|l_i(x)\|_2}$) at various layers in the architecture. Also, the relative change is shown for variants of our method that utilize the prior information about the training data distribution. Note that the percentage relative change in the feature activations due to the addition of the learned perturbation increases monotonically as we go deeper in the network. Because of this accumulated perturbation in the projection of the input, our learned adversaries are able to fool the CNNs independent of the task at hand. This phenomenon explains the fooling achieved by our objective. Also, Figure 12 shows that with the utilization of the data priors, the relative perturbation further increases. Hence, our objective achieves better fooling when the prior information is provided during the learning. Note that, for comparison, the baseline perturbation of random noise with equal max-norm as the learned perturbations is provided. The perturbation caused by the random noise is almost negligible at all the layers of CNN, which explains its robustness to random noise attacks.

Finally, we relate the relative change caused by our perturbations at the input to classification layer (f_{c_8} or softmax) to the fooling rates achieved for various perturbations. Table 10 shows the relative shift in the feature activations ($\frac{\|l_i(x+\delta)-l_i(x)\|_2}{\|l_i(x)\|_2}$) that are input to the classification layer and the corresponding fooling rates for various perturbations. Note that they are highly correlated, which explains why and how the proposed objective can fool the CNNs trained across multiple vision tasks.

6 CONCLUSION

In this paper, we proposed a novel data-free objective to craft image-agnostic (universal) adversarial perturbations (UAP). More importantly, we show that the proposed objective is generalizable not only across multiple CNN architectures but also across diverse computer vision tasks. We demonstrated that our seemingly simple objective of injecting maximal “adversarial” energy into the learned representations (subject to the imperceptibility constraint) is effective to fool both the classification and regression models. Significant transfer performances achieved by our

crafted perturbations can pose substantial threat to the deep learned systems in terms of black-box attacking.

Further, we show that our objective can exploit minimal priors about the target data distribution to craft stronger perturbations. For example, providing simple information such as the mean and dynamic range of the images to the proposed objective would craft significantly stronger perturbations. Though the proposed objective is data-free in nature, it can craft stronger perturbations when data is utilized.

More importantly, we introduced the idea of generalizable objectives to craft image-agnostic perturbations. It is already established that the representations learned by deep models are susceptible. On top of it, the existence of generic objectives to fool “any” learning based vision model independent of the underlying task can pose critical concerns about the model deployment. Therefore, it is an important research direction to be focused by the community in order to build reliable machine learning based systems.

REFERENCES

- [1] B. Biggio, G. Fumera, and F. Roli, “Pattern recognition systems under attack: Design issues and research challenges,” *International Journal of Pattern Recognition and Artificial Intelligence*, vol. 28, no. 07, 2014.
- [2] B. Biggio, I. Corona, D. Maiorca, B. Nelson, N. Šrndić, P. Laskov, G. Giacinto, and F. Roli, “Evasion attacks against machine learning at test time,” in *Joint European Conference on Machine Learning and Knowledge Discovery in Databases*, 2013, pp. 387–402.
- [3] L. Huang, A. D. Joseph, B. Nelson, B. I. Rubinstein, and J. D. Tygar, “Adversarial machine learning,” in *Proceedings of the 4th ACM Workshop on Security and Artificial Intelligence*, ser. AISec ’11, 2011.
- [4] C. Szegedy, W. Zaremba, I. Sutskever, J. Bruna, D. Erhan, I. J. Goodfellow, and R. Fergus, “Intriguing properties of neural networks,” *arXiv preprint arXiv:1312.6199*, 2013.
- [5] I. J. Goodfellow, J. Shlens, and C. Szegedy, “Explaining and harnessing adversarial examples,” *arXiv preprint arXiv:1412.6572*, 2014.
- [6] A. Kurakin, I. J. Goodfellow, and S. Bengio, “Adversarial machine learning at scale,” *arXiv preprint arXiv:1611.01236*, 2016.
- [7] S. Moosavi-Dezfooli, A. Fawzi, and P. Frossard, “Deepfool: A simple and accurate method to fool deep neural networks,” in *IEEE Computer Vision and Pattern Recognition (CVPR)*, 2016.
- [8] S. Moosavi-Dezfooli, A. Fawzi, O. Fawzi, and P. Frossard, “Universal adversarial perturbations,” in *IEEE Conference on Computer Vision and Pattern Recognition (CVPR)*, 2017.
- [9] K. R. Mopuri, U. Garg, and R. V. Babu, “Fast feature fool: A data independent approach to universal adversarial perturbations,” in *Proceedings of the British Machine Vision Conference (BMVC)*, 2017.
- [10] C. Xie, J. Wang, Z. Zhang, Y. Zhou, L. Xie, and A. Yuille, “Adversarial examples for semantic segmentation and object detection,” *arXiv preprint arXiv:1703.08603*, 2017.
- [11] J. H. Metzen, M. C. Kumar, T. Brox, and V. Fischer, “Universal adversarial perturbations against semantic image segmentation,” in *International Conference on Computer Vision (ICCV)*, 2017.
- [12] Y. Bengio, “Learning deep architectures for AI,” *Found. Trends Mach. Learn.*, vol. 2, no. 1, Jan. 2009.
- [13] N. Papernot, P. D. McDaniel, I. J. Goodfellow, S. Jha, Z. B. Celik, and A. Swami, “Practical black-box attacks against deep learning systems using adversarial examples,” *arXiv preprint arXiv:1602.02697*, 2016.
- [14] A. Kurakin, I. Goodfellow, and S. Bengio, “Adversarial examples in the physical world,” *arXiv preprint arXiv:1607.02533*, 2016.
- [15] C. Xie, J. Wang, Z. Zhang, Y. Zhou, L. Xie, and A. L. Yuille, “Adversarial examples for semantic segmentation and object detection,” *arXiv preprint arXiv:1703.08603*, 2017.
- [16] A. Fawzi, O. Fawzi, and P. Frossard, “Analysis of classifiers’ robustness to adversarial perturbations,” *arXiv preprint arXiv:1502.02590*, 2015.



Fig. 13. Sample failure case for the object recognition using VGG-16 model. Top row shows multiple clean images from ILSVRC validation set. Bottom row shows the adversarial images generated by adding the perturbation crafted utilizing the no data prior. Note that for all the shown images the perturbation fails to change the predicted label.



Fig. 14. Sample failure case for the semantic segmentation using the FCN-8s-VGG model. Top row shows the clean and corresponding perturbed images for no prior to various priors. Bottom row shows the predicted segmentation maps. Note that the people segments are undisturbed by the addition of various perturbations.

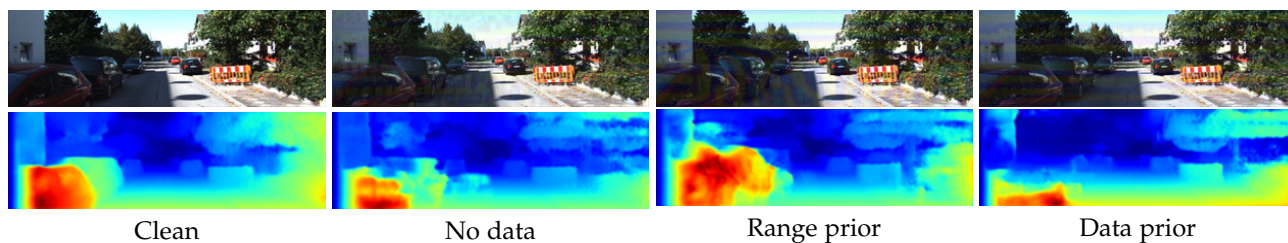


Fig. 15. Sample failure case for the depth estimation using Monodepth-VGG model. Note that, top row shows clean image and the corresponding perturbed images with no data case and various prior cases. Bottom row shows the corresponding depth predictions.

- [17] A. Fawzi, S. Moosavi-Dezfooli, and P. Frossard, "Robustness of classifiers: from adversarial to random noise," in *Advances in Neural Information Processing Systems (NIPS)*, 2016.
- [18] A. Nguyen, J. Yosinski, and J. Clune, "Deep neural networks are easily fooled: High confidence predictions for unrecognizable images," in *Computer Vision and Pattern Recognition (CVPR)*, 2015.
- [19] A. Rozsa, E. M. Rudd, and T. E. Boult, "Adversarial diversity and hard positive generation," in *Proceedings of the IEEE Conference on Computer Vision and Pattern Recognition (CVPR) Workshops*, 2016, pp. 25–32.
- [20] C. Xie, J. Wang, Z. Zhang, Y. Zhou, L. Xie, and A. Yuille, "Adversarial examples for semantic segmentation and object detection," in *International Conference on Computer Vision (ICCV)*, 2017.
- [21] V. Behzadan and A. Munir, "Vulnerability of deep reinforcement learning to policy induction attacks," *arXiv preprint arXiv:1701.04143*, 2017.
- [22] O. Bastani, Y. Ioannou, L. Lampropoulos, D. Vytiniotis, A. Nori, and A. Criminisi, "Measuring neural net robustness with constraints," in *Advances in Neural Information Processing Systems (NIPS)*, 2016.
- [23] A. Athalye, L. Engstrom, A. Ilyas, and K. Kwok, "Synthesizing robust adversarial examples," *arXiv preprint arXiv:1707.07397*, 2017.
- [24] C. Szegedy, W. Liu, Y. Jia, P. Sermanet, S. E. Reed, D. Anguelov, D. Erhan, V. Vanhoucke, and A. Rabinovich, "Going deeper with

- convolutions," *arXiv preprint arXiv:1409.4842*, 2014.
- [25] K. He, X. Zhang, S. Ren, and J. Sun, "Deep residual learning for image recognition," *arXiv preprint arXiv:1512.03385*, 2015.
- [26] O. Russakovsky, J. Deng, H. Su, J. Krause, S. Satheesh, S. Ma, Z. Huang, A. Karpathy, A. Khosla, M. Bernstein, A. C. Berg, and L. Fei-Fei, "ImageNet Large Scale Visual Recognition Challenge," *International Journal of Computer Vision (IJCV)*, vol. 115, no. 3, pp. 211–252, 2015.
- [27] M. Everingham, L. Van Gool, C. K. I. Williams, J. Winn, and A. Zisserman, "The PASCAL Visual Object Classes Challenge 2012 (VOC2012) Results."
- [28] M. Everingham, L. Van-Gool, C. K. I. Williams, J. Winn, and A. Zisserman, "The PASCAL Visual Object Classes Challenge 2007 (VOC2011) Results."
- [29] A. Geiger, P. Lenz, and R. Urtasun, "Are we ready for autonomous driving? the kitti vision benchmark suite," in *Conference on Computer Vision and Pattern Recognition (CVPR)*, 2012.
- [30] B. Zhou, A. Khosla, A. Lapedriza, A. Torralba, and A. Oliva, "Places: An image database for deep scene understanding," *arXiv preprint arXiv:1610.02055*, 2016.
- [31] D. P. Kingma and J. Ba, "Adam: A method for stochastic optimization," *arXiv preprint: arXiv:1412.6980*, 2014.
- [32] Y. Jia, E. Shelhamer, J. Donahue, S. Karayev, J. Long, R. Girshick, S. Guadarrama, and T. Darrell, "Caffe: Convolutional architecture for fast feature embedding," *arXiv preprint arXiv:1408.5093*, 2014.
- [33] K. Chatfield, K. Simonyan, A. Vedaldi, and A. Zisserman, "Return of the devil in the details: Delving deep into convolutional nets," in *Proceedings of the British Machine Vision Conference (BMVC)*, 2014.
- [34] K. Simonyan and A. Zisserman, "Very deep convolutional networks for large-scale image recognition," *arXiv preprint arXiv:abs/1409.1556*, 2014.
- [35] E. Shelhamer, J. Long, and T. Darrell, "Fully convolutional networks for semantic segmentation," *IEEE transactions on pattern analysis and machine intelligence (PAMI)*, vol. 39, no. 4, 2017.
- [36] L. C. Chen, G. Papandreou, I. Kokkinos, K. Murphy, and A. L. Yuille, "DeepLab: Semantic image segmentation with deep convolutional nets, atrous convolution, and fully connected CRFs," in *International Conference on Learning Representations (ICLR)*, 2015.
- [37] L.-C. Chen, G. Papandreou, I. Kokkinos, K. Murphy, and A. L. Yuille, "DeepLab: Semantic image segmentation with deep convolutional nets, atrous convolution, and fully connected crfs," *arXiv preprint arXiv:1606.00915*, 2016.
- [38] B. Hariharan, P. Arbeláez, L. Bourdev, S. Maji, and J. Malik, "Semantic contours from inverse detectors," in *IEEE International Conference on Computer Vision (ICCV)*, 2011.
- [39] C. Godard, O. Mac Aodha, and G. J. Brostow, "Unsupervised monocular depth estimation with left-right consistency," in *CVPR*, 2017.
- [40] D. B. Sam, S. Surya, and R. V. Babu, "Switching convolutional neural network for crowd counting," in *2017 IEEE Conference on Computer Vision and Pattern Recognition (CVPR)*, 2017.
- [41] A. Kendall and R. Cipolla, "Geometric loss functions for camera pose regression with deep learning," in *2017 IEEE Conference on Computer Vision and Pattern Recognition (CVPR)*, July 2017, pp. 6555–6564.
- [42] S. Song, F. Yu, A. Zeng, A. X. Chang, M. Savva, and T. Funkhouser, "Semantic scene completion from a single depth image," in *2017 IEEE Conference on Computer Vision and Pattern Recognition (CVPR)*, July 2017, pp. 190–198.
- [43] D. Xu, E. Ricci, W. Ouyang, X. Wang, and N. Sebe, "Multi-scale continuous crfs as sequential deep networks for monocular depth estimation," in *2017 IEEE Conference on Computer Vision and Pattern Recognition (CVPR)*, July 2017, pp. 161–169.
- [44] D. Eigen, C. Puhrsch, and R. Fergus, "Depth map prediction from a single image using a multi-scale deep network," in *Advances in Neural Information Processing Systems (NIPS)*, 2014, pp. 2366–2374.
- [45] C. Godard, O. Mac Aodha, and G. J. Brostow, "Unsupervised monocular depth estimation with left-right consistency," in *IEEE conference on Computer Vision and Pattern Recognition (CVPR)*, 2017.